Fish and Shellfish Immunology 87 (2019) 638–649

Contents lists available at ScienceDirect

Fish and Shellfish Immunology

journal homepage: www.elsevier.com/locate/fsi

Full length article

The activated β-integrin (*Cg*βV) enhances RGD-binding and phagocytic capabilities of hemocytes in *Crassostrea gigas*

Zhao Lv[a,b,c], Limei Qiu[a], Zhihao Jia[a,c], Weilin Wang[b,d], Zhaoqun Liu[d,e], Lingling Wang[d,e], Linsheng Song[b,d,e,*]

[a] Key Laboratory of Experimental Marine Biology, Institute of Oceanology, Chinese Academy of Sciences, Qingdao, 266071, China
[b] Laboratory of Marine Fisheries Science and Food Production Processes, Qingdao National Laboratory for Marine Science and Technology, Qingdao, 266235, China
[c] University of Chinese Academy of Sciences, Beijing, 100049, China
[d] Liaoning Key Laboratory of Marine Animal Immunology, Dalian Ocean University, Dalian, 116023, China
[e] Liaoning Key Laboratory of Marine Animal Immunology and Disease Control, Dalian Ocean University, Dalian, 116023, China

ARTICLE INFO

Keywords:
C. gigas
RGD-Binding
Integrin activation
Integrin-mediated phagocytosis

ABSTRACT

Integrins are an important family of cell receptors that can bind foreign particles and promote cell phagocytosis after they are activated. In the present study, a novel β integrin was identified from pacific oyster *Crassostrea gigas* with an extracellular domain, a single transmembrane segment, and a short cytoplasmic domain. It was phylogenetically clustered with phagocytosis-related insecta βV, and designated as *Cg*βV. *Cg*βV shared a conserved NPX[Y/F] motif related to integrin activation with other phagocytosis-related β integrins. The mRNA transcripts of *Cg*βV were widely detected in oyster tissues including hemocytes, gonad, adductor muscle, mantle, gill, and hepatopancreas, and the expression level in hemocytes was significantly up-regulated at 12 h after lipopolysaccharide (LPS) stimulation ($p < 0.05$), which was 2.29-fold higher than that in the control group. *Cg*βV proteins were mainly observed on the hemocytes surface. The oyster hemocytes were found to bind fluorescein isothiocyanate (FITC)-labeled Arg-Gly-Asp-containing peptides (RGDCPs), and the binding capability was significantly up-regulated with the peak percentage of 37.6% at 12 h post LPS stimulation, which was higher than that in the control group (8.8%, $p < 0.05$), suggesting the activation of RGD-binding integrins on oyster hemocytes surface. The label-free RGDCPs and anti-*Cg*βV antibody inhibited the binding capability of hemocytes towards FITC-labeled RGDCPs, which were significant lower in RGD blocking group (7.4%, $p < 0.05$) and anti-*Cg*βV blocking group (22.1%, $p < 0.05$) than that in the control group (37.6%), indicating that *Cg*βV could be a RGD-binding integrin. Phagocytosis assay demonstrated that LPS could enhance the phagocytosis of hemocytes towards *Escherichia coli* and fluorescent beads with the phagocytic rate (PR) of 18.3% and 17.4%, and phagocytic index (PI) of 5.29 and 37.71, respectively, which were significant higher than that in the control group (11.0% and 3.65 for *E. coli*, 9.8% and 29.26 for fluorescent beads, respectively, $p < 0.05$). In addition, both the label-free RGDCPs and anti-*Cg*βV antibody significantly hindered the phagocytosis of hemocytes towards *E. coli* and fluorescent beads. After the *E. coli* and fluorescent beads were opsonized by oyster serum, the label-free RGDCPs still inhibited the phagocytosis of hemocytes towards them, while the anti-*Cg*βV antibody could only inhibit the phagocytosis of hemocytes towards *E. coli*, suggesting that only the activated *Cg*βV was involved in the enhancing phagocytosis for bacteria in oyster. Moreover, the key components of conserved integrin-mediated phagocytosis pathway including GTPases, talin proteins, Ca^{2+} and cAMP were all induced by LPS in hemocytes of oyster. All these results suggested that the activated *Cg*βV enhanced RGD-binding and phagocytic capabilities of hemocytes, shedding lights on the mechanisms of integrin-mediated phagocytosis in mollusks.

1. Introduction

Integrins, a family of cell receptors, are heterodimers assembled by two distinct α and β subunits [1]. As important well known adhesion molecules, they are widely distributed on most cell surfaces to mediate cell-cell and cell-extracellular matrix (ECM) interactions, and participate in cell communication [2]. Evolutionarily, integrins are conserved in metazoans from sponges to humans, and function in multiple

* Corresponding author. Dalian Ocean University, 52 Heishijiao Street, Dalian, 116023, China.
E-mail address: lshsong@dlou.edu.cn (L. Song).

https://doi.org/10.1016/j.fsi.2019.01.047
Received 9 December 2018; Received in revised form 22 January 2019; Accepted 30 January 2019
Available online 10 February 2019
1050-4648/

physiological and pathological processes including immune responses, cell adhesion and migration, apoptosis, and tissue repair [3,4].

The interactions between integrins and ligands play crucial roles in integrin-mediated cellular processes [5]. In vertebrates, there are 18 α subunit genes and eight β subunit genes constituting at least twenty-four heterodimers [4]. According to the ligand types from ECM molecules, these twenty-four integrins can be classified into leucine-aspartic acid-valine (LDV)-binding receptors, Asp-Gly-Arg (RGD)-binding receptors, laminin receptors, and collagen receptors. The LDV-binding receptors bind the LDV containing peptides from laminins and collagens, while eight out of twenty-four integrins recognize the RGD-containing peptides (RGDCPs) in the native ligands such as collagens, fibronectins and certain laminin isoforms [1,6]. Upon ligands binding, the conformation of integrins changes, which could initiate multiple downstream signaling cascades associated with cellular immunity, cell motility, cell proliferation, and cell differentiation [2,6,7]. In invertebrates, the definitive number of integrin subunits is not well investigated, which has greatly impeded the study on α-β subunits pairing as well as integrin-ligand interaction. Recently, the accumulating evidences have revealed that RGDCPs can bind hemocytes and inhibit the cell activities in many invertebrates such as *Botryllus schlosseri* [8], *Pacifastacus leniusculus* [9], *Lymnaea stagnalis* [10], *Mytilus trossulus* [11], *C. gigas* [12] and etc., suggesting the existence of RGD-binding integrins in such animals.

In mammals, several integrins have been demonstrated to mediate cell phagocytosis. For example, integrin αMβ2 was identified as the first phagocytic integrin, which displayed an essential role in the uptake of complement-opsonized microorganisms and apoptotic cells in macrophages [13]. Mammalian integrin αVβ3 and αVβ5, the professional receptors for phagocytosis of apoptotic cells, can serve as opsonin receptors in cell phagocytosis [14]. In invertebrates, the studies on integrin-mediated phagocytosis are mainly focused on the roles of β subunits. For instances, shrimp β subunit can recognize the white spot syndrome virus (WSSV) envelope protein VP187 with the RGD motif, which provides the basis for specific engulfment of WSSV by hemocytes [15]. *Drosophila* β subunit acts as a receptor for bacterial cell wall components and apoptotic cells to promote the phagocytosis [16]. It is also reported that a β subunit in Chinese white shrimp *F. chinensis* serves as an opsonin receptor to interact with the hemolymph C-type lectin, and mediates opsonin-dependent phagocytosis [17]. The β subunits can directly recognize foreign targets and participate in opsonin-dependent phagocytosis, suggesting the diverse and complex roles of integrins in invertebrate phagocytosis.

It has been reported that mammalian phagocytosis-related integrins (αMβ2, αVβ3 and αVβ5) exist in at least three different conformations on phagocytes surface in the dynamic transformation [18]. The inactive integrins are folded over with a low binding affinity for ligands, and they do not involve in the signaling cascade. After integrins are primed, their activities are straightened to bind ligands with higher affinity. The activated integrins exhibit the highest affinity to bind ligands [6]. Exogenous lipopolysaccharide (LPS) is the activator for membrane integrins to induce the accumulation of intracellular GTPases (e.g., CDC-42, Ras, Rap-1). It is necessary and sufficient to prime ligand binding and phagocytic properties of extracellular part of integrin [18,19]. The intracellular part of integrin further recruits and phosphorylates talin proteins to induce the conformational change of integrin, which activates integrin to enhance the cell activities of ligand binding and phagocytosis [20,21]. In invertebrates, several different integrin signaling pathways in phagocytosis have been identified, such as α/CDC-42 pathway in *Caenorhabditis elegans* [22], β/Ras pathway in *Ceratitis capitate* [23], and β/MAPK pathway in medfly [24]. But the mechanisms of integrin activation and integrin-mediated phagocytosis are not well understood because of the lack of activation indicators and structural information.

As an important mollusk species inhabiting in intertidal zone, the pacific oyster *Crassostrea gigas* has evolved a set of sophisticated defense system, and phagocytosis is one of the most important immune reactions [25]. The recent released whole genome sequence of oyster provides useful information to understand its immune system [26], and the conserved functional elements or domains (GTPases, talin, and etc.) for integrin activation and integrin-mediated phagocytosis have been annotated referring to those in mammals [18,27]. In the present study, a novel β integrin (*Cg*βV) was identified from *C. gigas*, which could mediate phagocytosis as reported insecta βV. Its activation mechanism and role in phagocytosis were further investigated, hopefully to provide evidences for better understanding of integrin-mediated cell phagocytosis in mollusks.

2. Materials and methods

2.1. Experimental animals

Pacific oysters *C. gigas* (with 120–160 g in weight) were collected from an aquaculture farm in Qingdao, China and cultured in aerated water tank for one week before processing. Three five-week-old female Kunming mice were provided by the Qingdao Institute of Drug Control. All the experiments were approved by the Ethics Committee of the Institute of Oceanology, Chinese Academy of Sciences.

2.2. Immune stimulation and sample collection

After temporarily cultured, sixty oysters were divided into two groups. Thirty oysters stimulated with 100 μL of filtered seawater were used as the control group. The other thirty oysters received an injection with 100 μL of LPS (1 mg/mL) were used as experimental group. Six individuals were randomly sampled from each group at 0, 3, 6, 12 and 24 h post stimulation, and the hemolymph (1.0–1.5 mL per oyster) were collected from oyster hematococoel by using sterile syringe. The hemocytes and serum were separated by centrifugation at 800 *g*, 4 °C for 10 min. The tissues samples from unstimulated oyster tissues, including gill, mantle, adductor muscle, hepatopancreas, gonad and hemocytes, were collected to examine the distribution of *Cg*βV mRNAs.

2.3. RNA extraction and quantitative real-time PCR (qRT-PCR) analysis

Total RNA was extracted with Trizol reagent (Invitrogen), and the cDNA was synthesized by using M-MLV reverse transcriptase (Promega) according to the manufacturer's information. The mRNA expression level of *Cg*βV was detected by SYBR Green fluorescent *q*RT-PCR with the specific primers (Table 1) on ABI PRISM 7500 Sequence Detection System (Applied Biosystems). The *C. gigas* elongation factor (*Cg*EF) gene fragment was employed as the internal control [28]. The relative mRNA expression level of *Cg*βV was analyzed by comparative Ct method ($2^{-\triangle\triangle Ct}$ method) [29] (n = 6).

Table 1
Primers used in this study.

Primer purpose	Primer name	Sequence(5′-3′)
Clone primers	P1 (oligo (dT)-adaptor)	GGCCACGCGTCGACTAGTACT$_{17}$
	P2 (*Cg*βV-F)	CAACGTCTCAACGAGCTT
	P3 (*Cg*βV-R)	CCTATAACTTTCGCCGAT
RT primers	P4 (*Cg*βV-RT-F)	CCTTTATTCACCGCCTAT
	P5 (*Cg*βV-RT-R)	ATGTTGTTCTCCCTTGCT
	P6 (*Cg*EF-RTF)	AGTCACCAAGGCTGCACAGAAAG
	P7 (*Cg*EF-RTR)	TCCGACGTATTTCTTTGCGATGT
Recombination primers	P8 (*Cg*βV-Re-F)	GGAATTCCAACGTCTCAACGAGCTT
	P9 (*Cg*βV-Re-F)	CCGCTCGAGCCTATAACTTTCGCCGAT

Table 2
Species, proteins and GenBank accession numbers of β integrins used in phylogenetic reconstructions.

Species	Name	Accession
Caenorhabditis elegans	beta pat3	NP_497787.1
Biomphalaria glabrata	beta	AAC67503.1
Anopheles gambiae	beta int1	CAC00630.1
	betaV	AAM11657.1
Drosophila melanogaster	betaPS3	AAA28714.1
	betaV	NP_523608.2
Litopenaeus vannamei	beta-1	ADK56123.1
	beta-2	ACY82398.1
Crassostrea gigas	betaV	EKC35462.1
Nematostella vectensis	beta-1	XP_001641468
	beta-2	XP_001627336
	beta-3	XP_001637894
	beta-4	XP_001621822
Homo sapiens	beta1	CAD97649
	beta2	AAP88748
	beta3	AAA60122
	beta4	CAA37656
	beta5	AAP88764
	beta6	AAA36122
	beta7	AAB23688
	beta8	AAA36034

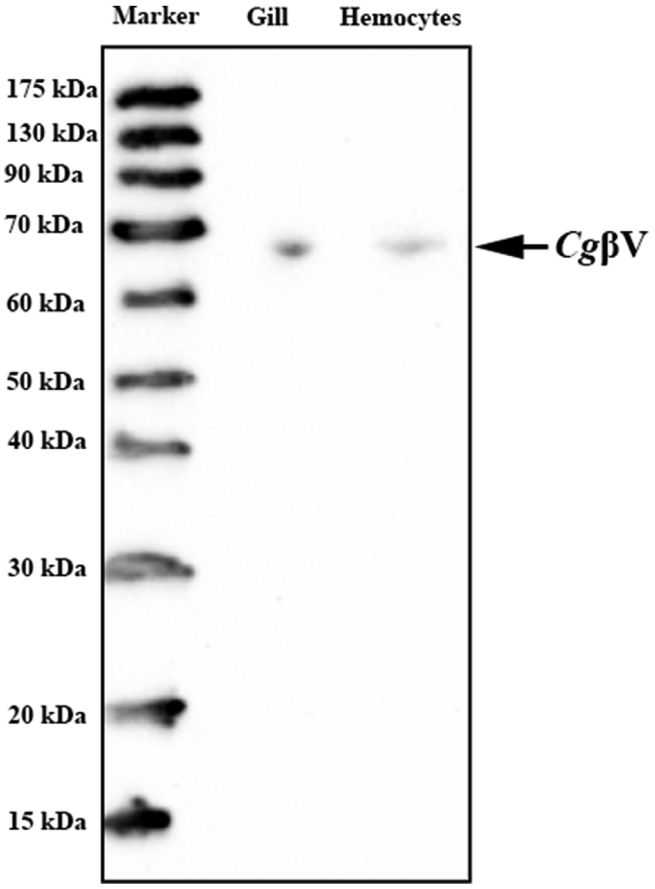

Fig. 1. Western blotting analysis of *Cg*βV proteins in gill and hemocytes.

2.4. Sequence analysis

The amino acid sequence of *Cg*βV (GenBank accession: EKC35462.1) was retrieved from NCBI (http://www.ncbi.nlm.nih.gov), and submitted to SMART (http://smart.embl-heidelberg.de/) to predicate the deduced protein domains. Multiple amino acid sequence alignments among *Cg*βV and five selected phagocytosis-related β integrins from human and *Drosophila* were conducted using Clustal Omega tool (http://www.ebi.ac.uk/Tools/msa/clustalo/), and the results were generated in the online platform (http://www.bio-soft.net/sms/) [30]. A phylogenetic tree was constructed by using MEGA 6.06 software with the neighbor-joining method based on all full-length β integrin protein sequences from different species (Table 2). A bootstrapping test was adopted with 1000 replications, and the phylogenetic tree was then edited online using iTOL tool (http://itol.embl.de/) [31].

2.5. Gene cloning and polyclonal antibody preparation

The cDNA fragment of 663 bp encoding the amino acids sequences from Q^{116} to R^{336} of *Cg*βV extracellular part was amplified by ExTaq DNA polymerase (Takara) with the specific cloning primers (Table 1). The PCR products were inserted into pMD19-T simple vector (Takara), and verified by nucleotide sequencing, and then integrated into pET-30a expression vector (Novagen), and expressed in *E. coli* Rosetta (DE3) system (TransGen Biotech). The Nickel-NTA Agarose column (Roche) chromatography was employed to purify His-tagged recombinant proteins according to the descriptions previously [32]. Subsequently, the purified recombinant *Cg*βV protein (r*Cg*βV) was dialyzed against TBS (50 mM Tris-HCl, 150 mM NaCl, pH 7.4) at 4 °C for three times, and the concentration was determined according to BCA assay kit (Sigma-Aldrich). The purified r*Cg*βV (1 μg/μL) was used to prepare mouse polyclonal antibody referring to the previous report [33]. After four immunizations with r*Cg*βV and adjuvant (Sigma-Aldrich), the serum of mouse was collected and then purified according to the protocol from IgG Purification Kit-G (Dojindo).

2.6. Western blotting analysis

Western blotting was employed to examine *Cg*βV proteins from hemocytes (5×10^6 cells) and gill post LPS stimulation at 12 h. After SDS-PAGE, the protein bands from hemocytes and gill were electrophoretically transferred onto nitrocellulose membrane and blocked in 5% skim milk powder solution. The membrane was incubated successively with the mouse anti-*Cg*βV antibody solution (diluted by 1:1000) at 4 °C overnight and 1:3000 (v/v) diluted HRP-conjugated goat-anti-mouse IgG (Abcam) at 4 °C for 2 h followed by thoroughly washing with TBST (50 mM Tris-HCl, 150 mM NaCl, 0.05% Tween-20, pH 7.4). Finally, the membranes were incubated in western lighting-ECL substrate system (Perkin Elmer) for imaging under ChemiDoc™ MP system (BIO-RAD).

2.7. Subcellular localization analysis

Immunofluorescence assay was performed to detect the subcellular localization of *Cg*βV proteins. The collected hemocytes were re-suspended in modified L-15 medium (0.54 g/L KCl, 20.2 g/L NaCl, 0.6 g/L $CaCl_2$, 3.9 g/L $MgCl_2$, 1 g/L $MgSO_4$) [34], and 20 μL of the re-suspension was seeded onto glass slides for cell adhesion. The hemocytes were fixed with 4% paraformaldehyde prepared in PBS (137 mmol/L NaCl, 2.7 mmol/L KCl, 10 mmol/L Na_2HPO_4, 2 mmol/L KH_2PO_4, pH 7.4) at room temperature for 15 min, and blocked by 3% BSA solution for 1 h. After washed three times with PBS, the hemocytes were incubated successively with anti-*Cg*βV antibody solution at a dilution of 1:250 for 1 h and Alexa Fluor 594-conjugated goat anti-mouse secondary antibody (Abcam) solution at a dilution of 1:250 for another 1 h. Finally, the cell nucleus was dyed with DAPI (Beyotime Biotech) for 5 min, and observed under a laser confocal scanning microscopy (Carl Zeiss LSM 710).

2.8. The detection of RGDCPs binding to hemocytes

The peptides RGDCPs (GRGDSP, 10 mg) and FITC labeled-RGDCPs (GRGDSP, 10 mg) with the purity of > 95% were synthesized by

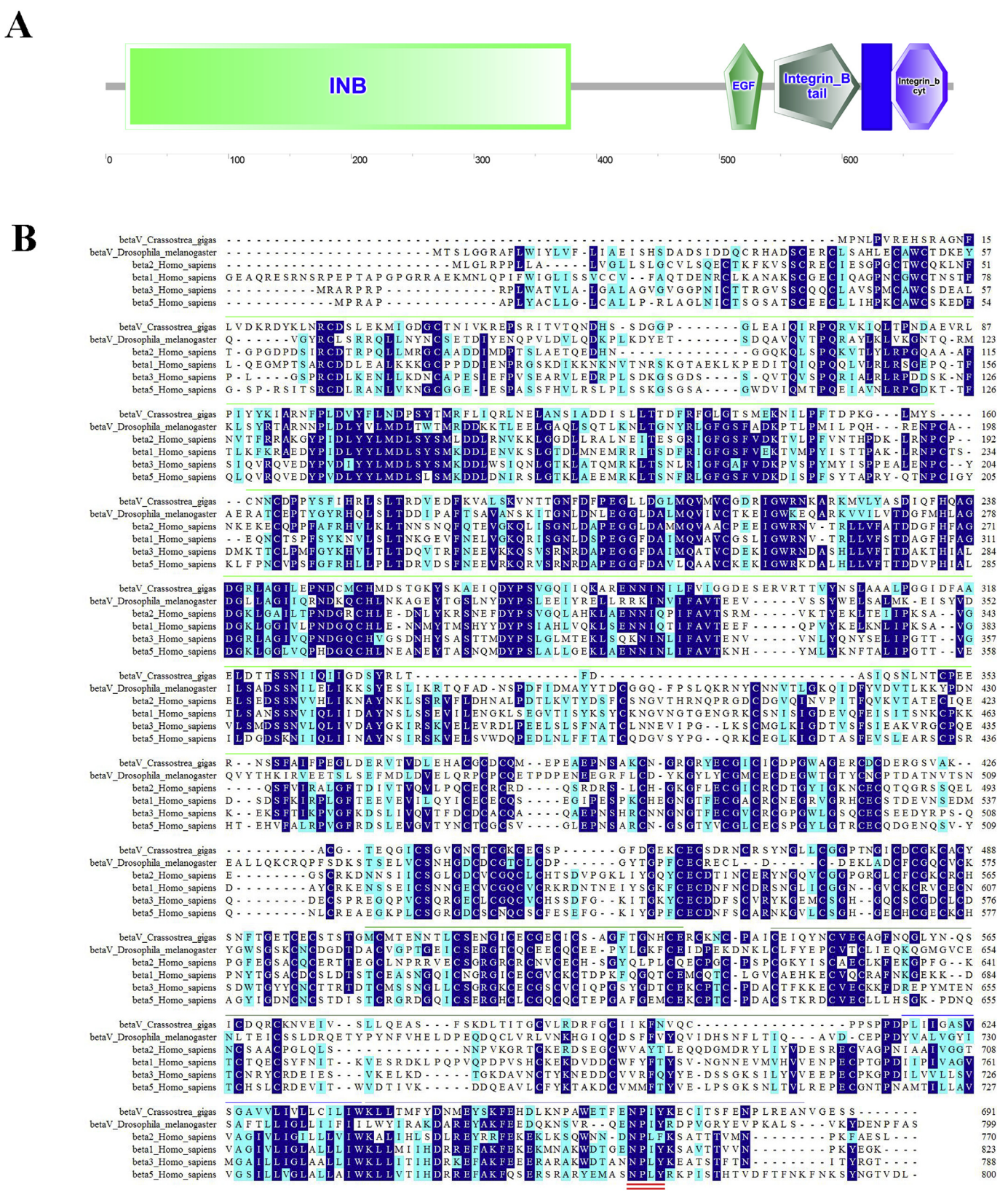

Fig. 2. Sequence features of *Cg*βV. (A) Prediction of protein domains by SMART analysis. (B) Multiple sequence alignments of *Cg*βV with known phagocytosis-related β integrins such as *Drosophila melanogaster* βV (NP_523608.2), *Homo sapien* β1 (CAD97649), *Homo sapien* β2 (AAP88748), *Homo sapien* β3 (AAA60122), *Homo sapien* β5 (AAP88764). The similar (consensus > 70%) and same amino acids are with light blue and dark blue background, respectively. Gaps are indicated by dashes to improve the alignment. (For interpretation of the references to color in this figure legend, the reader is referred to the Web version of this article.)

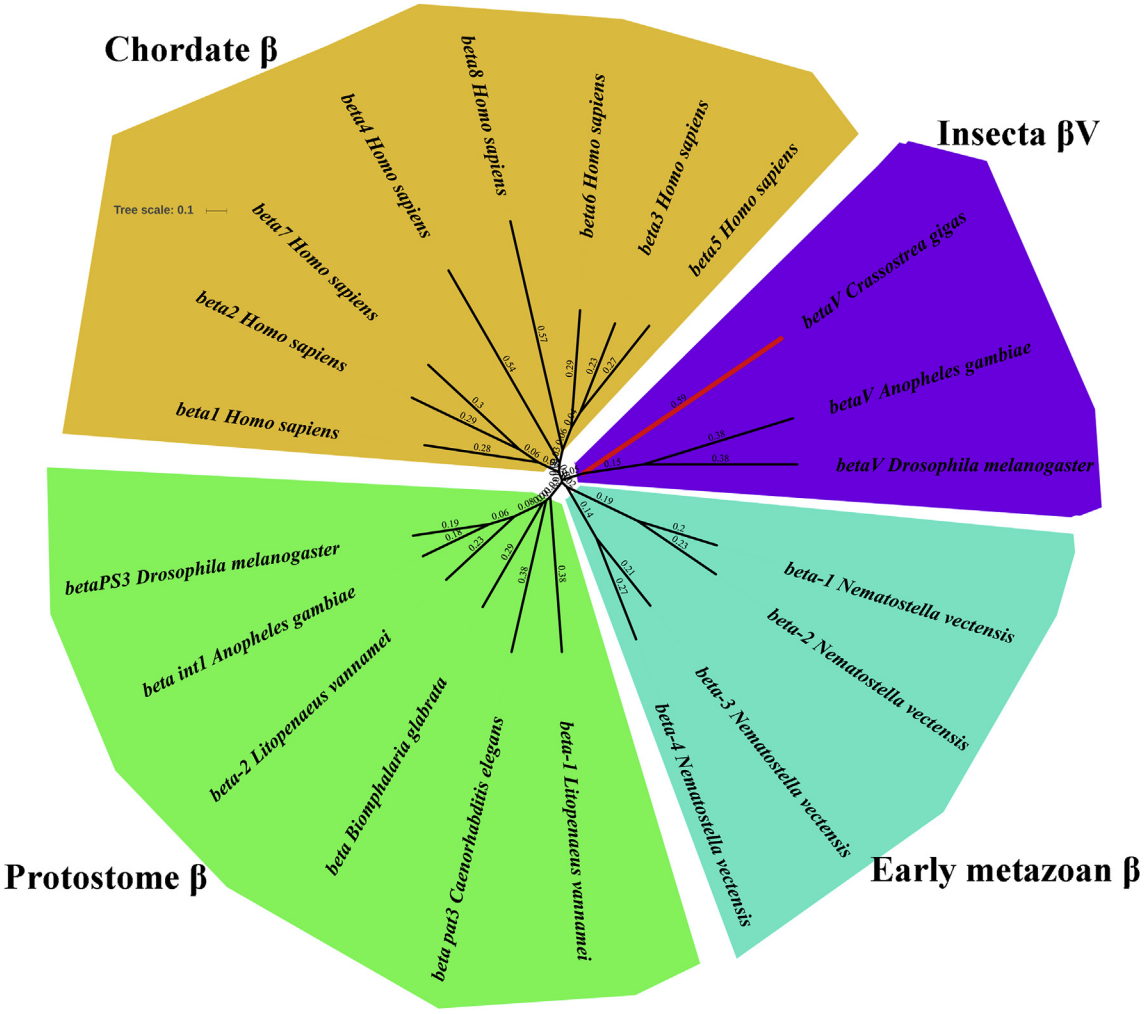

Fig. 3. Phylogenetic tree. Species, proteins and Genbank accession numbers of integrins used in phylogenetic reconstructions were listed in Table 2.

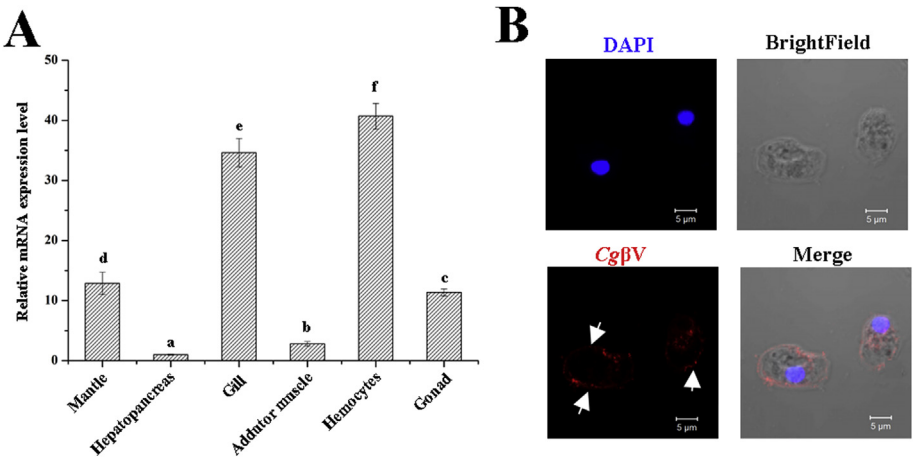

Fig. 4. The distribution of *Cg*βV mRNA transcripts in tissues and subcellular localization of *Cg*βV proteins. (A) Relative mRNA expression levels of *Cg*βV in different tissues. Results are shown as mean ± S.D. (n = 6), and the letters (a, b, c etc.) presented significant differences $p < 0.05$. (B) Localization of *Cg*βV protein in oyster hemocytes. *Cg*βV was visualized by Alexa 594-labeled secondary antibody (red color), and the nucleus of hemocytes were stained by DAPI (blue color). Bar = 5 μm. (For interpretation of the references to color in this figure legend, the reader is referred to the Web version of this article.)

Sangon Biotech (Shanghai, China). The collected hemocytes were re-suspended in modified L-15 medium (10^6 cells/mL), and then incubated with FITC labeled-RGDCPs (0.01 mg/mL) for 30 min. After extensive washing with modified L-15 medium, the hemocytes with FITC labeled-RGDCPs were fixed on glass slides and dyed with DAPI and observed under a laser confocal scanning microscopy (Carl Zeiss LSM 710). The percentage of hemocytes with FITC labeled-RGDCPs was determined by flow cytometry (BDFACSArial II). The label-free RGDCPs (0.01 mg/mL) and anti-*Cg*βV antibody (diluted by 1:50) were used to block the binding of hemocytes towards FITC labeled-RGDCPs, which were set as RGD blocking group and anti-*Cg*βV blocking group, respectively. There were three replicates for each sample.

2.9. The measurements of Ca^{2+} andcAMP levels

The level of Ca^{2+} was determined with fluorescence probe Rhod-2 AM (Thermo scientific, 1.0 μmol/L) according to the protocol. In brief, hemocytes (10^6 cells/mL) were incubated with the probes (5.0 μL) at

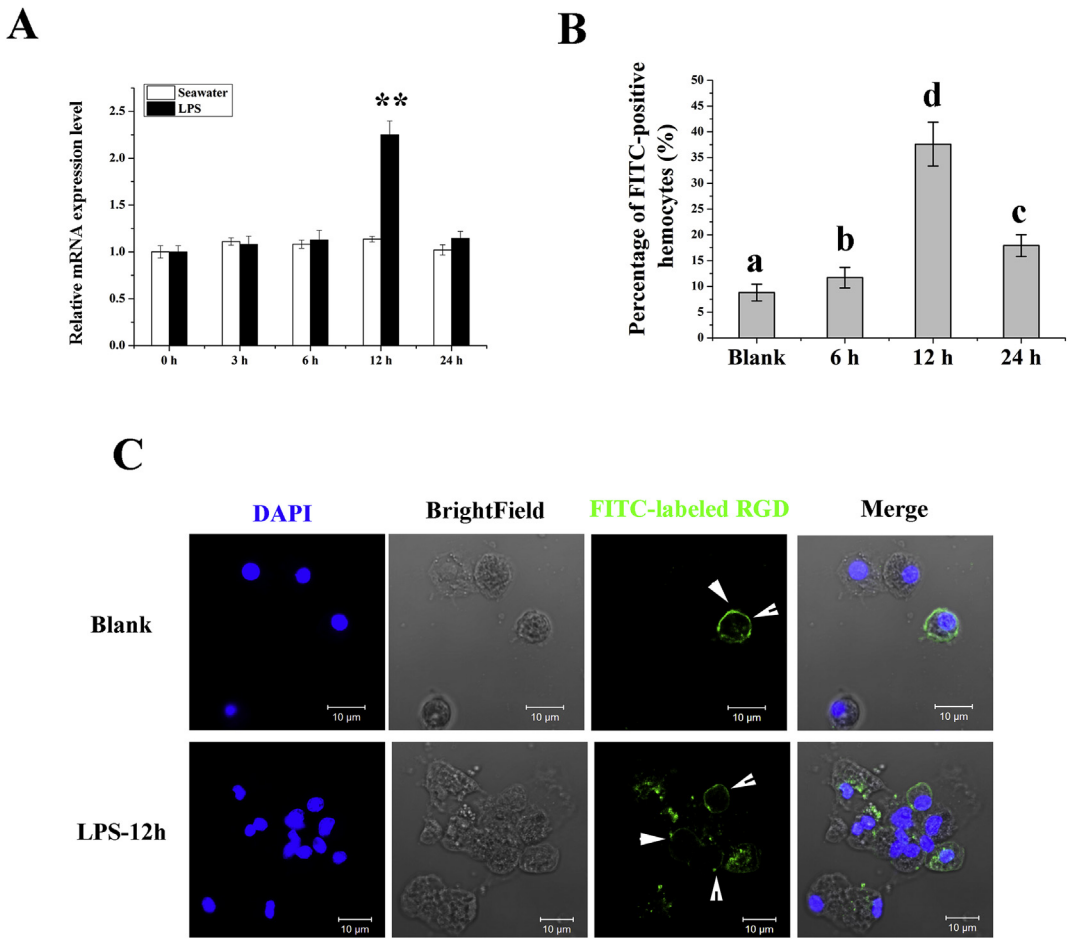

Fig. 5. The changes of *Cg*βV mRNA expression level and percentages of FITC-labeled RGDCPs hemocytes after LPS stimulation. (A) The temporal changes of *Cg*βV mRNA expression level in hemocytes post LPS and seawater stimulation. (B) Flow cytometry analysis about the percentage changes of FITC-positive hemocytes after LPS stimulation. Results are shown as mean ± S.D. (n = 3). The double asterisk (**) presented significant differences $p < 0.01$, and the letters (a, b, c etc.) presented significant differences $p < 0.05$. (C) Immunofluorescence analysis about FITC-positive hemocytes post LPS stimulation. The RGDCPs positive hemocytes was visualized by FITC fluorescence (green color), and the nucleus of hemocytes were stained by DAPI (blue color). Bar = 10 μm. (For interpretation of the references to color in this figure legend, the reader is referred to the Web version of this article.)

37 °C for 45 min and washed twice with modified L-15 medium. After centrifugation at 800 *g* for 10 min, the mean fluorescence intensity (MFI) of the cells was determined by flow cytometry (BDFACSArial II).

The concentration of cAMP was measured according to the instruction of cAMP Direct Immunoassay Kit (Abcam). The hemocytes were collected by centrifugation at 12,000 *g* for 10 min, and lysed completely by lysis reagent in the kit. The hemocyte lysates were centrifuged and the supernatant was collected as testing sample. The samples and the standard cAMP were neutralized and acetylated using the neutralizing buffer and acetylating reagent, respectively. For the quantification, 50 μL standard cAMP and testing samples were added into the Protein G coated 96-well plate. After blended by incubation with 10 μL cAMP antibody for 1 h, they were incubated with 10 μL cAMP-HRP for another 1 h with gentle agitation. After extensive washing, 100 μL of HRP developer was added into wells and incubated for 1 h. The reaction was then stopped by the addition of 100 μL of 1 mol/L HCl. The absorbance was detected by a microtiter plate reader (BioTek) at 450 nm. The background absorbance of the substrate was subtracted from all standards and samples. The molar concentration of cAMP in hemocytes was determined from standard curves generated by using standard cAMP [35].

2.10. The determination of talin protein levels and GTPase activity

The GTPase activity was determined referring to previous report [36]. GTPases hydrolyze GTP to release phosphate, and the released phosphate content can reflect the GTPase activity of hemocytes. Briefly, 10 μL of supernatant from hemocytes lysates as the testing sample (or 10 μL of assay buffer as negative control) was mixed with 20 μL assay buffer and 10 μL of guanosine triphosphate (GTP) (4 mM), and incubated at 37 °C for 30 min. Then, 200 μL of Stop Reagent was added into each well and incubated for an additional 30 min at room temperature to terminate the enzyme reaction and generate the colorimetric product. The absorbance values of the released phosphate were read at 620 nm for all samples.

Talin is an ancient and conserved protein found in organisms ranging from the amoebozoan protozoa to mammals [37]. The oyster talin protein was detected by commercial ELISA kit (CUSABIO) according to protocol of manufacturer. The final absorption value was determined at 450 nm by a microplate reader (BioTek). A relative quantitative method was used to reflect the changes in expression level of talin protein and GTPase activity in hemocytes. The OD values from stimulation groups were normalized to the control group. There were three replicates for each sample.

2.11. Phagocytosis assay

The bacteria (*E. coli*) were firstly fixed with absolute formaldehyde at room temperature for 10 min, and then washed three times with 0.1 M $NaHCO_3$ (pH 9.0). They were incubated with 1 mg/mL FITC

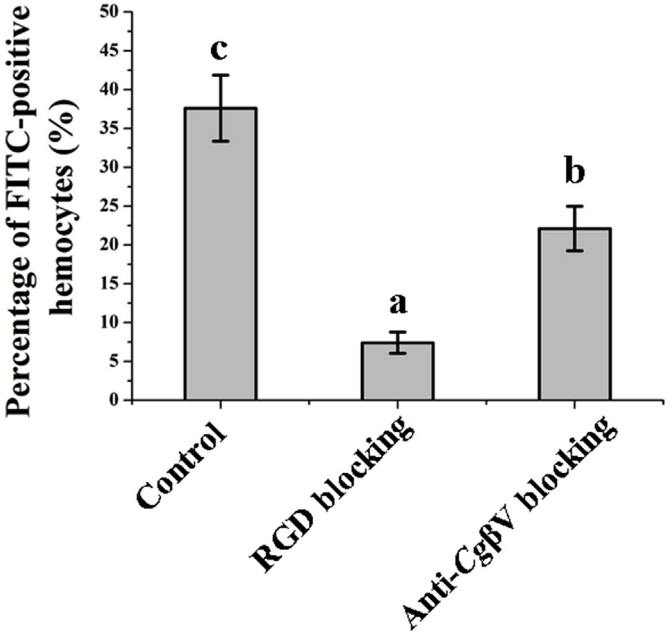

Fig. 6. The inhibition of hemocytes binding to FITC-labeled RGDCPs by RGDCPs or antibody. Results are shown as mean ± S.D. (n = 3), and the letters (a, b, c etc.) presented significant differences $p < 0.05$.

(Sigma-Aldrich) overnight to prepare FITC-labeled bacteria. In the phagocytosis assay without opsonization, hemocytes (10^6 cells/mL) were directly incubated with FITC-labeled *E. coli* (10^8 CFU/mL) and fluorescent yellow-green latex beads (Sigma-Aldrich, 2 μm, 10^8 beads/mL) at room temperature for 1 h with gentle rotation. For opsonic phagocytosis assay, FITC-labeled bacteria and fluorescent beads were previously incubated with oyster serum for 1 h, and then incubated with oyster hemocytes for cell phagocytosis. RGDCPs and anti-*Cg*βV antibody were used to block the corresponding integrins on hemocytes before the hemocytes were mixed with phagocytic particles. Pre-immune mouse serum and modified L-15 medium were used in negative control and blank group, respectively. The information of all treatment groups was listed in Table S1. The phagocytic activities of hemocytes from oysters stimulated with LPS or not were detected by flow cytometry (BDFACSArial II). The phagocytic rate (PR) and the phagocytic index (PI) were calculated by the percentage of hemocytes with fluorescence signals and the MFI of hemocytes, respectively [32]. There were three replicates for each sample.

2.12. Statistical analysis

All data were shown as mean ± S.D. The two-sample Student's *t*-test was performed for the comparisons between groups. Multiple group comparisons were executed by one-way ANOVA with a Tukey multiple group comparison test using PASW Statistics 18 software.

3. Results

3.1. The sequence characteristics of CgβV

The open reading frame (ORF) of *Cg*βV (GenBank accession: EKC35462.1) encoded a polypeptide of 691 amino acids with a predicted molecular mass of 76.29 kDa. Western blotting analysis revealed a specific protein band with the similar molecular mass from hemocytes or gill sample (Fig. 1). There were a large extracellular portion containing an N-terminal portion of extracellular INB domain, an EGF domain, an Integrin_B_tail domain, a single transmembrane segment and a short cytoplasmic Integrin_b_cyt domain in the deduced domains of *Cg*βV (Fig. 2A).

BLAST analysis revealed significant sequence similarity between *Cg*βV and five phagocytosis-related β integrins from human and insect. High conserved feature of NPX[Y/F] motif (residues $N^{668}PIY^{671}$ in *Cg*βV) was identified in cytoplasm segment near the transmembrane region of these β integrins, which were marked by double red underline in Fig. 2B. A phylogenetic tree of 21 selected β integrins from different species was constructed by the neighbor-joining method, and all the members were distinctly separated into four distinct groups including chordate β, protostome β, early metazoan β and insecta βV. *Cg*βV was clustered with *Anopheles gambiae* βV and *Drosophila melanogaster* βV, and assigned into the insecta βV group (Fig. 3).

3.2. The distribution of CgβV mRNA in tissues and subcellular localization of CgβV proteins

The expression levels of *Cg*βV mRNA in the different tissues were examined by *q*RT-PCR (Fig. 4A). The highest mRNA expression level of *Cg*βV was detected in hemocytes, which was 40.69-fold of that in hepatopancreas ($p < 0.05$). The mRNA expression levels of *Cg*βV was relatively higher in gill (34.62-fold of that in hepatopancreas, $p < 0.05$), while lower in mantle, gonad and adductor muscle with 12.88-fold ($p < 0.05$), 11.37-fold ($p < 0.05$) and 2.82-fold ($p < 0.05$) of that in hepatopancreas, respectively (Fig. 4A).

Immunofluorescence assay was performed to detect the subcellular localization of *Cg*βV proteins in oyster hemocytes. *Cg*βV, indicated by Alexa Fluor 594-conjugated antibody, was observed in the red color, which was mainly localized on the hemocytes membrane (Fig. 4B).

3.3. The expression pattern of CgβV mRNA in hemocytes after LPS stimulation

The expression of *Cg*βV mRNA in hemocytes was examined by *q*RT-PCR at 0, 3, 6, 12, and 24 h after LPS stimulation. The mRNA expression level of *Cg*βV was only upregulated at 12 h, which was 2.29-fold ($p < 0.05$) of that in the control group (seawater treatment group). No significant change was detected at other time-points post LPS stimulation (Fig. 5A).

3.4. The enhanced binding activity of hemocytes towards RGDCPs induced by LPS

The percentage of hemocytes with FITC-labeled RGDCPs after LPS stimulation was determined by flow cytometry to evaluate the activation of RGD-binding integrins. No significant difference in the percentages of hemocytes with positive signals of FITC was observed between the seawater stimulation group and the blank group (data not shown). The percentage of hemocytes with FITC signals was about 8.8% in the blank group (before LPS stimulation), while it increased to 11.7% ($p < 0.05$), 37.6% ($p < 0.05$), and 17.9% ($p < 0.05$) at 6, 12 and 24 h post LPS stimulation, respectively (Fig. 5B).

The positive signals of FITC could be visually observed under confocal scanning microscopy (Fig. 5C). The percentage of hemocytes with FITC signals peaked at 12 h post LPS stimulation, indicating the possible activation of RGD-binding integrins. The hemocytes samples stimulated by LPS for 12 h were selected for blockage experiments with label-free RGDCPs and anti-*Cg*βV antibody. The percentage of hemocytes with FITC signals in RGD blocking group was significantly lower than that in the control group (7.4% vs. 37.6%, $p < 0.05$). It was 22.1% in anti-*Cg*βV blocking group, which was significantly lower than that in the control group (37.6%, $p < 0.05$) and significantly higher than that in RGD blocking group (7.4%, $p < 0.05$) (Fig. 6).

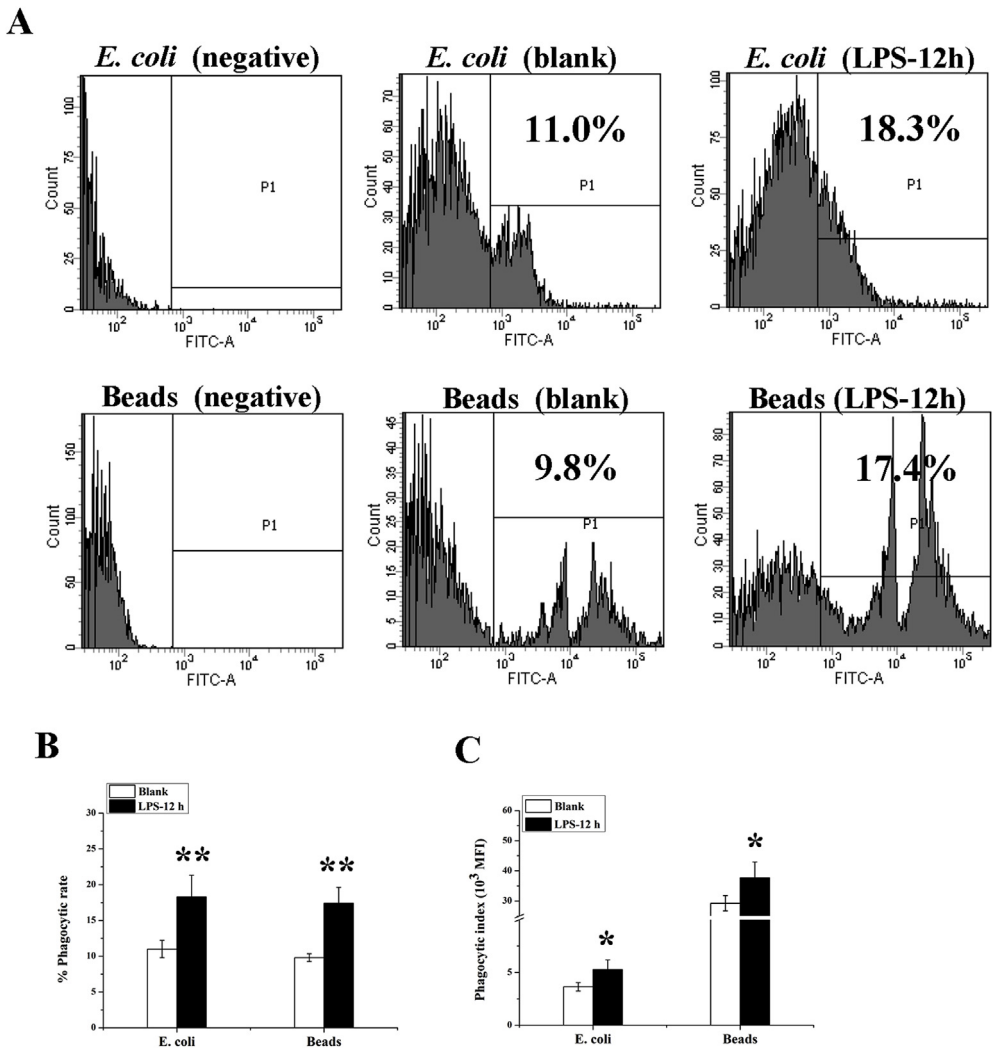

Fig. 7. The changes of hemocytic phagocytic activity after LPS stimulation. (A) Flow cytometry analysis about the changes of phagocytic activity after LPS stimulation. (B) The changes of phagocytic rate. (C) The changes of phagocytic index. Results are mean ± S.D. (n = 3), and the single or double asterisk (* or **) presented significant differences $p < 0.05$ or $p < 0.01$.

3.5. The enhanced phagocytic capabilities of oyster hemocytes induced by LPS

The phagocytic capabilities of oyster hemocytes stimulated by LPS stimulation for 12 h were determined to investigate the functions of integrins. The PRs towards FITC-labeled *E. coli* and yellow-green latex beads were significantly upregulated to 18.3% ($p < 0.05$) and 17.4% ($p < 0.05$) after LPS stimulation, which were significant higher than 11.0% for *E. coli* and 9.8% for beads in the control group without LPS stimulation, respectively (Fig. 7). The PIs were also increased significantly with the MFI values of 5.29 towards *E. coli* ($p < 0.05$) and 37.71 towards beads ($p < 0.05$) in LPS group, compared to 3.65 (*E. coli*) and 29.26 (beads) in the control group (Fig. 7), respectively.

The phagocytosis of the LPS stimulated hemocytes were also detected after they were blocked by RGDCPs and anti-*Cg*βV antibodies to reveal the possible roles of *Cg*βV in phagocytosis. The PR of hemocytes towards FITC-labeled *E. coli* not opsonized by oyster serum was 18.3% (Blank + NOp group), which was significantly higher than 11.5% (RGD blocking + NOp group, $p < 0.05$) in the group blocked by RGDCPs and 14.5% (Anti-*Cg*βV blocking + NOp group, $p < 0.05$) in the group blocked by anti-*Cg*βV antibodies, respectively (Fig. 8A). The PI of hemocytes was significantly decreased from 5.29 (Blank + NOp group) to 3.81 (RGD blocking + NOp group, $p < 0.05$) and 4.26 (Anti-*Cg*βV blocking + NOp group, $p < 0.05$) after the hemocytes were blocked by RGDCPs and anti-*Cg*βV antibodies, respectively (Fig. 8B).

After the FITC-labeled *E. coli* was opsonized by oyster serum, the PR of hemocytes significantly increased from 18.3% (Blank + NOp group) to 27.8% (Blank + Op group) ($p < 0.05$), while it significantly decreased from 27.8% (Blank + Op group) to 20.3% (RGD blocking + Op group, $p < 0.05$) and 24.9% (Anti-*Cg*βV blocking + Op group, $p < 0.05$) after the hemocytes were blocked by RGDCPs and anti-*Cg*βV antibodies, respectively (Fig. 8A). The PI of hemocytes significantly increased from 5.29 (Blank + NOp group) to 6.73 (Blank + Op group, $p < 0.05$) after FITC-labeled *E. coli* was opsonized by oyster serum, while it decreased significantly from 6.73 (Blank + Op group) to 4.23 (RGD blocking + Op group, $p < 0.05$) and 5.64 (Anti-*Cg*βV blocking + Op group, $p < 0.05$) after the hemocytes were blocked by RGDCPs and anti-*Cg*βV antibodies, respectively (Fig. 8B). In addition, the PR towards FITC-labeled *E. coli* was 20.3% (RGD blocking + Op group) after the hemocytes were blocked by RGDCPs, which was significantly lower than that of 24.9% (Anti-*Cg*βV blocking + Op group, $p < 0.05$) after the hemocytes were blocked by anti-*Cg*βV antibodies (Fig. 8A) The PI towards FITC-labeled *E. coli* was also significantly lower in RGD blocking + Op group than that in Anti-*Cg*βV blocking + Op group (4.23 vs. 5.64, $p < 0.05$) (Fig. 8B).

After the beads were opsonized, no significant differences in PRs were observed in Blank + Op group compared to Blank + NOp group (16.9% vs. 17.4%, $p > 0.05$). The anti-*Cg*βV antibodies could not

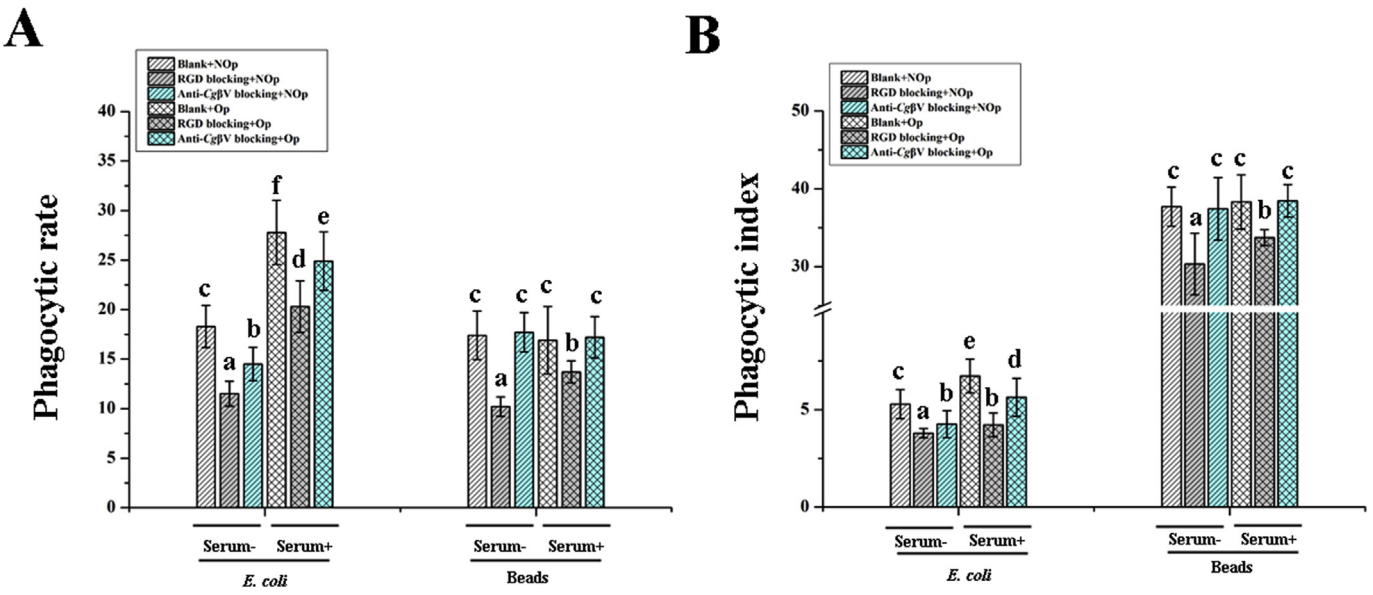

Fig. 8. The inhibition of hemocytic phagocytic activity by RGDCPs or antibodies. (A) The changes of phagocytic rate and (B) phagocytic index towards *E. coli* and beads after oposonization or not. Results are mean ± S.D. (n = 3), and the letters (a, b, c etc.) presented significant differences $p < 0.05$. The information of all treatment groups was listed in Table S1.

inhibit the phagocytic capabilities towards beads whether they were opsonized by oyster serum or not, and no significant differences in PRs were observed between Anti-*Cg*βV blocking + NOp group and Blank + NOp group (17.7% vs. 17.4%, $p > 0.05$), and between Anti-*Cg*βV blocking + Op group and Blank + Op group (17.2% vs. 17.7%, $p > 0.05$) (Fig. 8A). Similarly, no significant differences of PIs were observed between Blank + Op group and Blank + NOp group (38.32 vs. 37.71, $p > 0.05$), between Anti-*Cg*βV blocking + NOp group and Blank + NOp group (37.43 vs. 37.71, $p > 0.05$), and between Anti-*Cg*βV blocking + Op group and Blank + Op group (38.37 vs. 37.43, $p > 0.05$) (Fig. 8B).

RGDCPs significantly inhibited the phagocytic capabilities. The PR in RGD blocking + NOp group was 10.2% ($p < 0.05$), which was lower than 17.4% in Blank + NOp group when the beads were not opsonized by oyster serum. The PR in RGD blocking + Op group (13.7%, $p < 0.05$) also decreased to 16.9% in Blank + Op group when the beads were opsonized by oyster serum (Fig. 8A). The PI towards the beads not opsonized by oyster serum significantly decreased from 37.71 (Blank + NOp group) to 30.34 (RGD blocking + NOp group, $p < 0.05$), and the PI towards the beads opsonized by oyster serum decreased from 38.32 (Blank + Op group) to 33.76 (RGD blocking + Op group, $p < 0.05$) after the hemocytes were blocked by RGDCPs (Fig. 8B).

3.6. The changes of GTPase activity and levels of talin protein, Ca^{2+} and cAMP levels after LPS stimulation

GTPases and talin protein as the upstream activators in the integrins-mediated phagocytosis, and secondary messengers Ca^{2+} and cAMP as downstream targets were selectively detected in the present study (Fig. 9). The GTPase activity in hemocytes increased significantly, which was 3.74-fold ($p < 0.05$), 2.31-fold ($p < 0.05$) and 2.06-fold ($p < 0.05$) of that in the control at 6, 12, and 24 h post LPS stimulation, respectively (Fig. 9A). The expression levels of talin protein in hemocytes also increased significantly to 2.78-fold ($p < 0.05$), 2.14-fold ($p < 0.05$) and 1.55-fold ($p < 0.05$) at 6, 12, and 24 h post LPS stimulation, respectively, compared to that in the control (Fig. 9A).

The cAMP level in hemocytes increased significantly after LPS stimulation. It was 11.46 pmol/mg protein ($p < 0.05$) at 12 h post LPS stimulation, which was higher than that in the control (9.67 pmol/mg protein). No significant changes in cAMP level of hemocytes were detected at other time-points post LPS stimulation (Fig. 9B). The Ca^{2+} level in hemocytes was detected by flow cytometry using specific probes, and it increased significantly with the MFI values of 87.1 ($p < 0.05$), 124.0 ($p < 0.05$) and 93.3 ($p < 0.05$) at 6, 12 and 24 h after LPS stimulation, respectively, which were higher than that in the control with the MFI value of 57.7 (Fig. 9C).

4. Discussion

Integrins are a family of transmembrane molecules that play crucial roles in cell-cell and cell-ECM interactions, which are mostly considered in the context of cell adhesion and migration [18,38]. In the present study, a β integrin (*Cg*βV) was identified in *C. gigas* and it was phylogenetically clustered with insecta βV involved in cell phagocytosis. A large extracellular portion, a single transmembrane segment and a short cytoplasmic domain were predicted in *Cg*βV, which could participate in the binding of extracellular molecules and triggering the intracellular signaling pathways to regulate immune responses as most reported β integrins [12]. Multiple sequence alignments revealed that there was a conserved motif of NPX[Y/F] in the cytoplasmic segment near transmembrane region of *Cg*βV. The NPX[Y/F] motif is only absent in β4 and β8 of human integrins, and it is necessary and sufficient for the activation of phagocytosis-related β integrins (β1, β2, β3 and β5) and integrin-mediated phagocytosis [18]. The existences of NPX[Y/F] motif in the predicted structure of *Cg*βV indicated its functions in oyster phagocytosis.

As cell receptors, integrins can transduce multiple cell signals through the interactions with extracellular ligands [5,6]. In human, the whole integrin family of twenty-four members can be typically classified into LDV-binding receptors, RGD-binding receptors, laminin receptors and collagen receptors in terms of their ligands [1,4]. Eight out of them including α5β1, α8β1, αVβ1, αVβ3, αVβ5, αVβ6, αVβ8 and αIIbβ3 belong to RGD-binding receptors, and they are demonstrated to be involved in cellular immunity, cell motility, cell proliferation, and cell differentiation [39]. In the present study, the synthetic RGDCPs conjugated with FITC was observed to bind oyster hemocytes, and the antibody of *Cg*βV could partly block the binding of FITC-labelled RGDCPs to oyster hemocytes, demonstrating that *Cg*βV possibly existed as a RGD-binding integrin in oyster. In invertebrates, accumulating

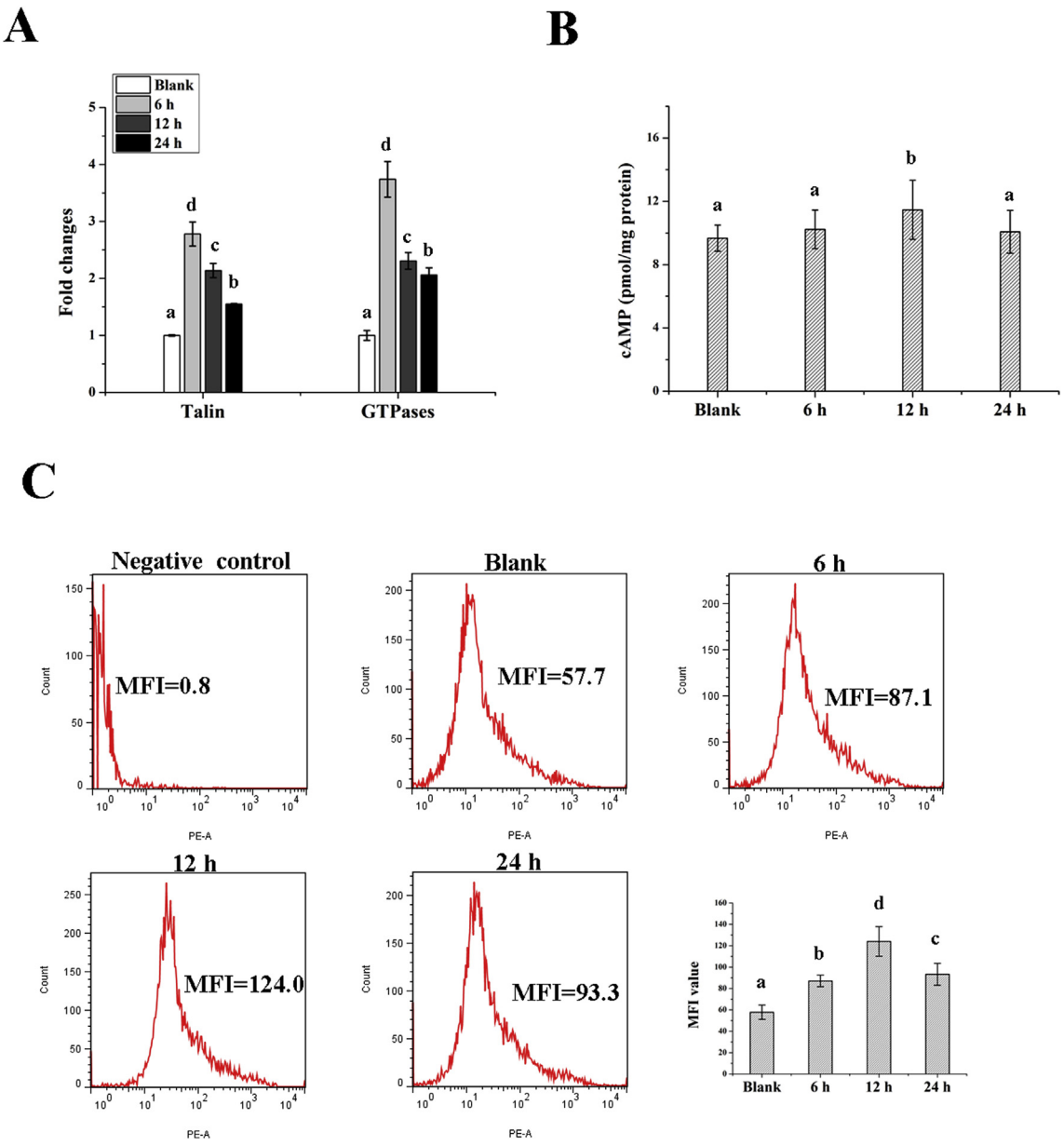

Fig. 9. The changes of molecular activities in integrin-mediated phagocytosis pathway after LPS stimulation. (A) The fold changes of talin protein level and GTPases activity in hemocytes. (B) The changes of cAMP concentration in hemocytes. (C) The changes of Ca^{2+} level in hemocytes. Results are mean ± S.D. (n = 3), and the letters (a, b, c etc.) presented significant differences $p < 0.05$.

evidences have revealed that RGD-binding integrin can mediate multiple cell processes. For example, in primitive invertebrate *Hydra*, RGD-binding integrin has been proved as one molecular mechanism for amoeboid cell locomotion [40]. The RGD-binding integrins are also involved in hemocytes adhesion during cell cultivation in mussel *Mytilus trossulus* [11], and directly mediate cell phagocytosis for foreign invasions in many invertebrates [8,9,12]. The phagocytosis of big agents has been reported to mainly rely on macropinocytosis-dependent endocytosis where the host cytoplasmic membrane sags to coat the big agents and ingests them into cell [41,42]. Bacteria always secrete many kinds of molecules on their surface to bind the specific phagocytic receptor on host cell surface and initiate phagocytosis [43]. In the present study, the antibody of *Cg*βV could significantly hinder the cell phagocytosis for bacteria, while it could not significantly hinder the cell phagocytosis for fluorescent latex beads (2 μm), indicating that *Cg*βV was only involved in the phagocytosis of *E. coli* but not beads in *C. gigas*. It could be explained reasonably by the previous reports about *Ceratitis capitata* phagocytosis that bacteria carried with integrin-binding sites and beads without integrin-binding sites [23]. However, the binding sites of *E. coli* towards *Cg*βV remained to be further investigated. In addition, the hindrance of *Cg*βV antibody on cell phagocytosis for bacteria was weaker than that of RGDCPs ($p < 0.05$). It was speculated that there could be multiple RGD-binding integrins in oyster, and *Cg*βV was one of RGD-binding integrins to mediate phagocytosis.

Integrins commonly mediate cell phagocytosis with the assistance of opsonins, which can bind to the invading targets and then interact with integrins on cell surface [8]. In mammals, αMβ2 is primarily expressed on macrophages and neutrophils, which can bind C3bi-coated invading microbes in serum to initiate the complement-dependent phagocytosis [13]. In invertebrates, α subunit α_{Hr1} from ascidian *Halocynthia roretzi* is found to be involved in the complement-mediated phagocytic activities of hemocytes, which is similar as the α subunits of CR3 and CR4 in vertebrates [44]. Recently, RNA-seq analysis indicated a potential multi-component complement system in oyster *C. gigas*, and many

complement molecules such as C-type lectins and C1qDCs were demonstrated with opsonic functions in hemolymph, although the opsonin receptors were not identified [32,45–47]. In the present study, the oyster hemocytes preferred to engulf the bacteria pre-incubated with serum rather than the untreated bacteria, indicating that certain molecules could serve as opsonins for bacteria in oyster serum, and *Cg*βV could be the opsonin receptor because the blockage of *Cg*βV significantly inhibited cell phagocytosis for the bacteria treated with serum.

In mammals, most phagocytic integrins exist in three major allosteric conformations, inactive (low-affinity state), primed (moderate-affinity state) and active (high-affinity state) [7]. The inactive integrins have low binding affinity for ligands, which can be experimentally activated by exogenous LPS via 'inside-out' signal to activate integrins with the highest affinity to bind ligands and mediate effective phagocytosis [7,18]. In invertebrates, integrins or integrin-like molecules from sipunculan worm *Themiste petricola* have been demonstrated to be activated by LPS to enhance phagocytosis by fluorescence assays using anti-human CD14, CD11B and CD11C antibodies. But the indicators of integrin activation have not well been established [48]. In the present study, the phagocytosis of oyster hemocytes was enhanced by LPS stimulation, and the enhanced binding capacity of hemocytes to RGDCPs was also detected, which should be the indicators of RGD-binding integrin activation. Furthermore, the enhanced binding capacity of hemocytes to RGDCPs and the significant upregulation of *Cg*βV mRNA in hemocytes were both observed at 12 h post LPS stimulation, suggesting the activation of *Cg*βV as one of RGD-binding integrins in oyster.

In mammals, the activation of αMβ2 greatly depends on the accumulation of GTPase Rap1 in macrophages, which controls 'inside-out' signaling [49]. The binding of a cytoskeletal protein talin to the conserved motif of NPX[Y/F] in the cytoplasmic tail of β2 is a common final step in its activation process to activate the downstream pathway [50]. Although there is no αMβ2 identified in invertebrates, α subunit/GTPase CDC-42 pathway and β subunit/GTPase Ras pathway have been identified in *C. elegans* [22] and *C. capitate* [23], respectively. The involvement of *Cg*βV in the modulation of phagocytosis, prompted us to elucidate the molecular mechanisms of its activation in phagocytosis. In the present study, total level of GTPase activity and the content of potential talin proteins both peaked at 6 h post LPS stimulation, which were earlier than the peak time of the enhanced binding capacity of hemocytes to RGDCPs or the activation of *Cg*βV at 12 h post LPS stimulation. The accumulation of GTPases and talin proteins in hemocytes should be the upstream events of *Cg*βV activation, which were also reported in the activation of αMβ2 to enhance cell phagocytosis in mammals [18]. Ca^{2+} and cAMP level are demonstrated as important messenger molecules, and they have been speculated as the downstream of integrin activation as reported previously in mammals [51,52]. In the present study, the levels of Ca^{2+} and cAMP in hemocytes increased significantly after LPS stimulation and peaked at 12 h post stimulation. Therefore, the mechanisms of *Cg*βV activation to enhance hemocytic phagocytosis in oyster might be related to the conserved molecular activities of intracellular GTPases, talin proteins, Ca^{2+}, and cAMP.

Taken together, a novel membranal β integrin (*Cg*βV) was identified in *C. gigas*, with a large extracellular INB domain, a single transmembrane segment and a short cytoplasmic domain with the conserved motif of NPX[Y/F]. It was phylogenetically clustered with phagocytosis-related insecta βV. *Cg*βV mRNA transcripts could be widely detected in oyster tissues, and its mRNA expression level in hemocytes was greatly induced by LPS. *Cg*βV were mainly localized on the hemocytes surface as a RGD-binding integrin, and the binding of hemocytes to RGDCPs could be facilitated by LPS. In addition, *Cg*βV could mediate hemocytic phagocytosis for bacteria with RGD-dependence and serum-dependence, and the phagocytosis could be facilitated by LPS partly based on the activation of membranal *Cg*βV. The activation of *Cg*βV might be associated with the conserved molecular activities of intracellular GTPases, talin proteins, Ca^{2+} and cAMP. These results provided solid evidences to clarify the activation mechanism and the roles of *Cg*βV in oyster phagocytosis, shedding lights on the defense mechanisms via integrin-mediated phagocytosis in mollusks.

Acknowledgements

The authors are grateful to all the laboratory members for continuous technical advice and helpful discussions. This research was supported by the National Natural Science Foundation of China (No. U1706204, 31530069), earmarked fund (CARS-49) from Modern Agro-industry Technology Research System, AoShan Talents Cultivation Program Supported by Qingdao National Laboratory for Marine Science and Technology (No. 2017ASTCP-OS13), Dalian High Level Talent Innovation Support Program (2015R020), and the Research Foundation for Talented Scholars in Dalian Ocean University (to L. S.).

Appendix A. Supplementary data

Supplementary data to this article can be found online at https://doi.org/10.1016/j.fsi.2019.01.047.

References

[1] M. Barczyk, S. Carracedo, D. Gullberg, Integrins. Cell Tissue Res. 339 (2010) 269–280.
[2] F.G. Giancotti, E. Ruoslahti, Integrin signaling, Science 285 (1999) 1028–1032.
[3] A.L. Hughes, Evolution of the integrin alpha and beta protein families, J. Mol. Evol. 52 (2001) 63–72.
[4] R.O. Hynes, Integrins: bidirectional, allosteric signaling machines, Cell 110 (2002) 673–687.
[5] D. Kiyozumi, R. Sato-Nishiuchi, K. Sekiguchi, In situ detection of integrin ligands, Curr. Protoc. Cell Biol. 65 (2014) 1–7.
[6] I.D. Campbell, M.J. Humphries, Integrin structure, activation, and interactions, Cold Spring Harb. Perspect. Biol. (2011) 3.
[7] I.M. Olsen, C. Ffrench-Constant, Dynamic regulation of integrin activation by intracellular and extracellular signals controls oligodendrocyte morphology, BMC Biol. 3 (2005) 25.
[8] L. Ballarin, M. Scanferla, F. Cima, A. Sabbadin, Phagocyte spreading and phagocytosis in the compound ascidian *Botryllus schlosseri*: evidence for an integrin-like, RGD-dependent recognition mechanism, Dev. Comp. Immunol. 26 (2002) 345–354.
[9] M.W. Johansson, Cell adhesion molecules in invertebrate immunity, Dev. Comp. Immunol. 23 (1999) 303–315.
[10] L.D. Plows, R.T. Cook, A.J. Davies, A.J. Walker, Integrin engagement modulates the phosphorylation of focal adhesion kinase, phagocytosis, and cell spreading in molluscan defence cells, B. B. A-Mol. Cell Res. 1763 (2006) 779–786.
[11] M.A. Maiorova, N.A. Odintsova, Beta Integrin-like protein-mediated adhesion and its disturbances during cell cultivation of the mussel *Mytilus trossulus*, Cell Tissue Res. 361 (2015) 581–592.
[12] Z. Jia, T. Zhang, S. Jiang, M. Wang, Q. Cheng, M. Sun, et al., An integrin from oyster *Crassostrea gigas* mediates the phagocytosis toward *Vibrio splendidus* through LPS binding activity, Dev. Comp. Immunol. 53 (2015) 253–264.
[13] D.M. Underhill, A. Ozinsky, Phagocytosis of microbes: complexity in action, Annu. Rev. Immunol. 20 (2002) 825–852.
[14] S. Akakura, S. Singh, M. Spataro, R. Akakura, J.I. Kim, M.L. Albert, et al., The opsonin MFG-E8 is a ligand for the alphavbeta5 integrin and triggers DOCK180-dependent Rac1 activation for the phagocytosis of apoptotic cells, Exp. Cell Res. 292 (2004) 403–416.
[15] D.F. Li, M.C. Zhang, H.J. Yang, Y.B. Zhu, X. Xu, Beta-integrin mediates WSSV infection, Virology 368 (2007) 122–132.
[16] S. Nonaka, K. Nagaosa, T. Mori, A. Shiratsuchi, Y. Nakanishi, Integrin alphaPS3/betanu-mediated phagocytosis of apoptotic cells and bacteria in *Drosophila*, J. Biol. Chem. 288 (2013) 10374–10380.
[17] X.W. Wang, X.F. Zhao, J.X. Wang, C-type lectin binds to beta-integrin to promote hemocytic phagocytosis in an invertebrate, J. Biol. Chem. 289 (2014) 2405–2414.
[18] A.G. Dupuy, E. Caron, Integrin-dependent phagocytosis: spreading from micro-adhesion to new concepts, J. Cell Sci. 121 (2008) 1773–1783.
[19] A. Aderem, D.M. Underhill, Mechanisms of phagocytosis in macrophages, Annu. Rev. Immunol. 17 (1999) 593–623.
[20] S.J. Shattil, C. Kim, M.H. Ginsberg, The final steps of integrin activation: the end game, Nat. Rev. Mol. Cell Biol. 11 (2010) 288.
[21] D.A. Calderwood, Talin controls integrin activation, Biochem. Soc. T. 32 (2004) 434.
[22] H.H. Hsieh, T.Y. Hsu, H.S. Jiang, Y.C. Wu, Integrin alpha PAT-2/CDC-42 signaling is required for muscle-mediated clearance of apoptotic cells in *Caenorhabditis elegans*, PLoS Genet. 8 (2012) e1002663.
[23] L.C. Foukas, H.L. Katsoulas, N. Paraskevopoulou, A. Metheniti, M. Lambropoulou, V.J. Marmaras, Phagocytosis of *Escherichia coli* by insect hemocytes requires both

activation of the Ras/mitogen-activated protein kinase signal transduction pathway for attachment and beta3 integrin for internalization, J. Biol. Chem. 273 (1998) 14813–14818.
[24] I. Mamali, I. Lamprou, F. Karagiannis, M. Karakantza, M. Lampropoulou, V.J. Marmaras, A beta integrin subunit regulates bacterial phagocytosis in medfly haemocytes, Dev. Comp. Immunol. 33 (2009) 858–866.
[25] L. Wang, X. Song, L. Song, The oyster immunity, Dev. Comp. Immunol. 80 (2018) 99–118.
[26] G. Zhang, X. Fang, X. Guo, L. Li, R. Luo, F. Xu, et al., The oyster genome reveals stress adaptation and complexity of shell formation, Nature 490 (2012) 49–54.
[27] T. Zhang, L. Qiu, Z. Sun, L. Wang, Z. Zhou, R. Liu, et al., The specifically enhanced cellular immune responses in Pacific oyster (*Crassostrea gigas*) against secondary challenge with *Vibrio splendidus*, Dev. Comp. Immunol. 45 (2014) 141–150.
[28] Y. Du, L. Zhang, F. Xu, B. Huang, G. Zhang, L. Li, Validation of housekeeping genes as internal controls for studying gene expression during Pacific oyster (*Crassostrea gigas*) development by quantitative real-time PCR, Fish. Shellfish Immun. 34 (2013) 939–945.
[29] K.J. Livak, T.D. Schmittgen, Analysis of relative gene expression data using real-time quantitative PCR and the 2(-Delta Delta C(T)) Method, Methods 25 (2001) 402–408.
[30] P. Stothard, The sequence manipulation suite: JavaScript programs for analyzing and formatting protein and DNA sequences, Biotechniques 28 (2000) 4 1102.
[31] I. Letunic, P. Bork, Interactive Tree of Life (iTOL): an online tool for phylogenetic tree display and annotation, Bioinformatics 23 (2007) 127–128.
[32] Z. Lv, L. Qiu, M. Wang, Z. Jia, W. Wang, L. Xin, et al., Comparative study of three C1q domain containing proteins from pacific oyster *Crassostrea gigas*, Dev. Comp. Immunol. 78 (2018) 42–51.
[33] J. Xu, S. Jiang, Y. Li, M. Li, Q. Cheng, D. Zhao, et al., Caspase-3 serves as an intracellular immune receptor specific for lipopolysaccharide in oyster *Crassostrea gigas*, Dev. Comp. Immunol. 61 (2016) 1–12.
[34] A. Cao, L. Mercado, J.I. Ramos-Martinez, R. Barcia, Primary cultures of hemocytes from *Mytilus galloprovincialis* Lmk.: expression of IL-2Rα subunit, Aquaculture 216 (2003) 1–8.
[35] X. Wang, M. Wang, Z. Jia, H. Wang, S. Jiang, H. Chen, et al., Ocean acidification stimulates alkali signal pathway: a bicarbonate sensing soluble adenylyl cyclase from oyster *Crassostrea gigas* mediates physiological changes induced by CO2 exposure, Aquat. Toxicol. 181 (2016) 124–135.
[36] Y. Chi, F. Li, Y. Sun, R. Wen, S. Li, Expression and function analysis of Rac1 homolog in Chinese shrimp *Fenneropenaeus chinensis*, Fish. Shellfish Immun. 35 (2013) 927–932.
[37] M.A. Senetar, R.O. McCann, Gene duplication and functional divergence during evolution of the cytoskeletal linker protein talin, Gene 362 (2005) 141–152.
[38] S.M. Albelda, C.A. Buck, Integrins and other cell adhesion molecules, FASEB J. 4 (1990) 2868–2880.
[39] J. Takagi, Structural basis for ligand recognition by RGD (Arg-Gly-Asp)-dependent integrins, Biochem. Soc. T. 32 (2004) 403–406.
[40] U. Ziegler, R.P. Stidwill, The attachment of nematocytes from the primitive invertebrate *Hydra* to fibronectin is specific and RGD-dependent, Exp. Cell Res. 202 (1992) 281–286.
[41] Y. Li, L. Sun, J. Li, Macropinocytosis-dependent endocytosis of Japanese flounder IgM+ B cells and its regulation by CD22, Fish. Shellfish Immun. 84 (2019) 138–147.
[42] Y. Li, L. Sun, J. Li, Internalization of large particles by turbot (*Scophthalmus maximus*) IgM+ B cells mainly depends on macropinocytosis, Dev. Comp. Immunol. 82 (2018) 31–38.
[43] L.M. Stuart, R.A. Ezekowitz, Phagocytosis: elegant complexity, Immunity 22 (2005) 539–550.
[44] S. Miyazawa, K. Azumi, M. Nonaka, Cloning and characterization of integrin alpha subunits from the solitary ascidian, *Halocynthia roretzi*, J. Immunol. 166 (2001) 1710–1715.
[45] L. Wang, H. Zhang, L. Wang, D. Zhang, Z. Lv, Z. Liu, et al., The RNA-seq analysis suggests a potential multi-component complement system in oyster *Crassostrea gigas*, Dev. Comp. Immunol. 76 (2017) 209–219.
[46] H. Li, H. Zhang, S. Jiang, W. Wang, L. Xin, H. Wang, et al., A single-CRD C-type lectin from oyster *Crassostrea gigas* mediates immune recognition and pathogen elimination with a potential role in the activation of complement system, Fish. Shellfish Immun. 44 (2015) 566–575.
[47] S. Jiang, H. Li, D. Zhang, H. Zhang, L. Wang, J. Sun, et al., A C1q domain containing protein from *Crassostrea gigas* serves as pattern recognition receptor and opsonin with high binding affinity to LPS, Fish. Shellfish Immun. 45 (2015) 583–591.
[48] G.A. Blanco, A.M. Escalada, E. Alvarez, S. Hajos, LPS-induced stimulation of phagocytosis in the sipunculan worm *Themiste petricola*: possible involvement of human CD14, CD11B and CD11C cross-reactive molecules, Dev. Comp. Immunol. 21 (1997) 349–362.
[49] S. Sayedyahossein, L. Dagnino, Integrins and small GTPases as modulators of phagocytosis, Int. Rev. Cel. Mol. Bio. 302 (2013) 321–354.
[50] K.L. Wegener, A.W. Partridge, J. Han, A.R. Pickford, R.C. Liddington, M.H. Ginsberg, et al., Structural basis of integrin activation by talin, Cell 128 (2007) 171–182.
[51] S. Koutsogiannaki, M. Kaloyianni, Effect of 17beta-estradiol on adhesion of *Mytilus galloprovincialis* hemocytes to selected substrates. Role of alpha2 integrin subunit, Fish. Shellfish Immun. 31 (2011) 73–80.
[52] K.B. Uribe, C. Martin, A. Etxebarria, D. Gonzalez-Bullon, G. Gomez-Bilbao, H. Ostolaza, Ca2+ influx and tyrosine kinases trigger *Bordetella* adenylate cyclase toxin (ACT) endocytosis. Cell physiology and expression of the CD11b/CD18 integrin major determinants of the entry route, PLoS One 8 (2013) e74248.